Electronic Supplementary Information (ESI)

Discrete polygonal supramolecular architectures of isocytosine-based Pt(II) complexes at the solution-graphite interface

Mohamed El Garah,[§] Stephan Sinn,[¥] Arezoo Dianat,[#] Alejandro Santana-Bonilla,[#] Rafael Gutierrez,[#] Luisa De Cola,[¥,] Gianaurelio Cuniberti,[*,#,†,‡] Artur Ciesielski,[§] and Paolo Samorì[*,§]

[§]Laboratoire de Nanochimie, ISIS & icFRC, Nanochenistry, Université de Strasbourg & CNRS, 8 allée Gaspard Monge, 67000 Strasbourg, France.
E-mail: samori@unistra.fr

[¥]Laboratoire de chimie et biomateriaux supramolecilaire, ISIS & icFRC, Nanochenistry, Université de Strasbourg & CNRS, 8 allée Gaspard Monge, 67000 Strasbourg, France.

[#]Institute for Materials Sciences and Max Bergmann Center of Biomaterials, TU Dresden, 01062 Dresden, Germany.
[†]Dresden Center for Computational Materials Science (DCCMS), TU Dresden, 01062 Dresden, Germany.
[‡]Center for Advancing Electronics Dresden, TU Dresden, 01062 Dresden, Germany.
E-mail: projects@tu-dresden.de

Table of content

1. **Synthesis**……..……...……..S3

1.1 Synthesis of Py-CF3-2H……..…..…..…..S3

1.2 Synthesis of 4-isoCytosinyl-pyridine…….……S3

1.3 Synthesis of Pt-CF_3-DMSO …….…..…...…S4

1.4 *Synthesis of Pt-CF3-Py-iCyt* ..……...…..…….S5

2. **Photophysical properties** ……..……..…… ……S7

3. **Scanning Tunneling Microscopy**…….……..……...…S8

3.*1 Experimental section*……..S8

3.2 Self-assembly of Pyridine-isocytosine……..…….…….....S9

4. **DFT calculation**……...……..…S12

4.1 *Molecular Structures*……...……S12

4.2 *Molecular orbitals*……...….....…S14

4.3 *Re-arrangement energies* ……...……..…...…...…...…S14

5. **References**……..……...……...……S15

1. Synthesis

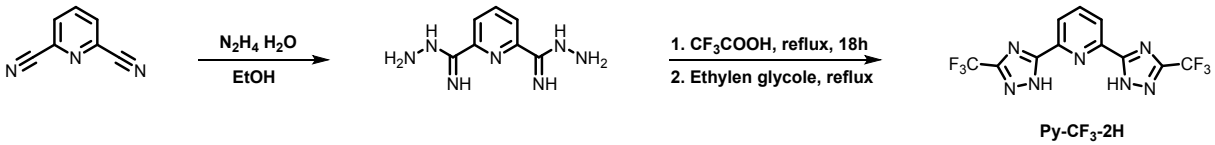

1.1 Synthesis of Py-CF3-2H

Following the literature in parts[1], pyridine-2,6-dicarbonitrile (5 g, 39 mmol) was dissolved in EtOH (140 mL). To this, Hydrazine monohydrate (65%, 30 mL, 402 mmol) was added, which led to an immediate precipitation. The reaction mixture was stirred for 24 h at ambient temperature and subsequently the solvents were evaporated *in vacuo* to obtain a white solid, which in turn was dissolved in trifluoroacetic acid (50 mL, 653 mmol). This mixture was heated to 80°C for 18h and afterwards concentrated *in vacuo*. Ethylene glycol (50 mL) was added and the mixture heated to 140 °C for 2 h. After cooling down to ambient temperature, the product was precipitated in an excess of a mixture of water (400 mL). After Buchner filtration the solid was recrystallized from acetone to yield X-ray suitable crystals (5.181 g, 14.8 mmol, 38%).

^{1}H NMR (400 MHz, THF) δ 10.26 (s, 2H), 9.03 (d, ^{3}J = 6.4 Hz, 4H), 7.95 (t, ^{3}J = 7.9 Hz, 2H), 7.52 – 7.37 (m, 4H), 7.31 (d, J = 7.8 Hz, 4H), 4.56 – 4.42 (m, 4H), 4.40 (d, J = 1.7 Hz, 2H), 4.21 – 4.03 (m, 4H), 3.98 – 3.80 (m, 6H), 3.80 – 3.65 (m, 6H). ^{19}F {^{1}H} NMR (377 MHz, THF) δ -66.79 (s). HR-ESI-MS (positive scan, *m/z*): $[M+Na]^{+}$ calcd. 1635.2107; found 1635.2200

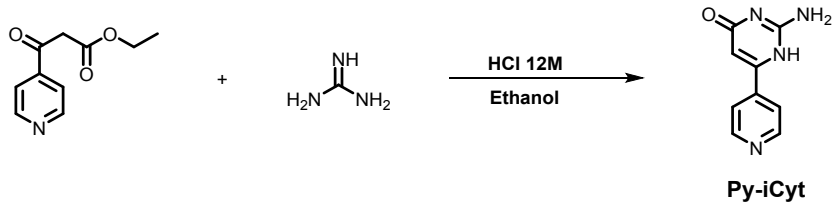

*1.2 Synthesis of 4-isoCytosinyl-pyridine (***Py-iCyt***)*

Ethyl 3-oxo-3-(pyridin-4-yl)propanoate (707 mg, 3.66 mmol) and Guanidine carbonate (2.4 g, 5.49 mmol) were suspended in absolute ethanol (10 mL) in an inert atmosphere. Subsequently, aqueous HCl (12 M, 110 µL) were added and the reaction mixture heated to

reflux for 18h. The reaction mixture was allowed to cool to room temperature and precipitate filtered through Buchner filtration. The solid was thoroughly washed with ethanol and diethylether and afterwards transferred to a round bottom flask and dissolved in aqueous NaOH (1 M, 12 mL). This solution was heated to reflux for 2h and subsequently acidified with glacial acetic acid (3 mL). The resulting precipitate was filtered through a Buchner filtration, washed with distilled water, ethanol, diethylether and subsequently dried under ambient condition to yield a white solid (54 mg, 0.28 mmol, 8%).

^{1}H NMR (400 MHz, DMSO) δ 10.89 (s, 1H), 8.50 (d, *J* = 6.1 Hz, 2H), 7.72 (d, *J* = 6.1 Hz, 2H), 6.59 (s, 2H), 6.12 (s, 1H). HR-ESI-MS (positive scan, *m/z*): $[M+H]^+$ calcd. 189.0771; found 189.0765.

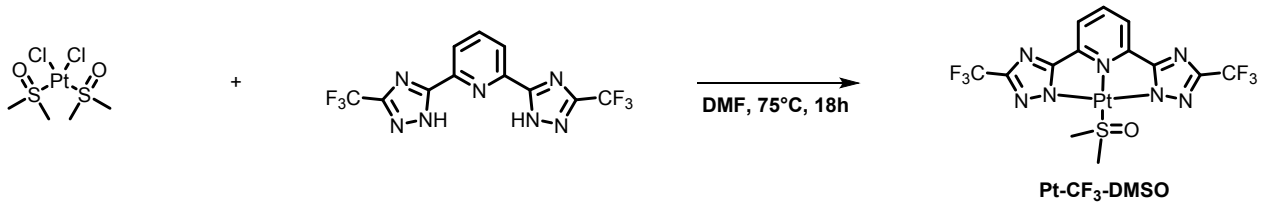

Pt-CF_3-DMSO

1.3 Synthesis of CF_3-Pt- DMSO

$PtDMSO_2Cl_2$ (419 mg, 0.99 mmol) and **Py-CF_3-2H** (213 mg, 0.99 mmol) were dissolved in DMF and heated to 75 °C in a round bottom equipped with a reflux condenser overnight. The reaction mixture was allowed to cool to room temperature and the volatiles removed *in vacuo*. The crude product was subsequently distributed in DCM, sonicated and afterwards centrifuged. The supernatant was taken off the solid and this procedure was repeated once with DCM and another time with MeOH to obtain a pure red solid (390 mg, 0.629 mmol, 64 %).

^{1}H NMR (400 MHz, MeOD) δ 8.26 (s, 1H), 7.89 (d, *J* = 7.9 Hz, 2H), 2.71 (s, 6H). ^{19}F {^{1}H} NMR (377 MHz, MeOD) δ -65.66 (s). HR-ESI-MS (positive scan, *m/z*): $[M+Na]^+$ calcd. 643.0071; found 643.0034.

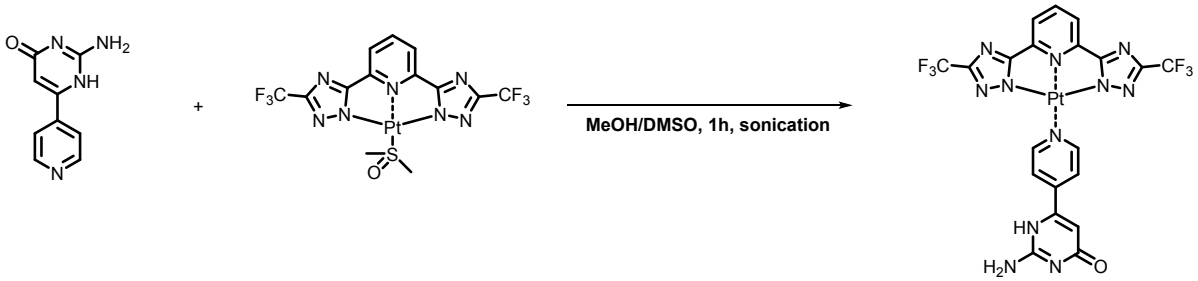

Pt-CF_3-Py-iCyt

1.4 Synthesis of CF_3-Pt- Py-iCyt

CF_3-Pt- DMSO (6.7 mg, 0.01 mmol) and Py-iCyt (2 mg, 0.01 mmol) were dissolved in a mixture of MeOH/DMSO (2 mL, 10:1, *v,v*) and sonicated for 1 hour in a closed Eppendorf vial leading to the formation of a yellow emissive precipitate. Subsequently, the crude product mixture was centrifuged and the supernatant taken off. The solid was afterwards treated with THF and subsequently again centrifuged to receive the solid. This procedure was repeated with MeOH two times and one time with THF to obtain a pure solid product (8 mg, 0.008 mmol, 82%), which appears orange after the treatment with THF.

^{1}H NMR (400 MHz, THF) δ 10.38 (s, 1H), 9.79 (d, J = 6.3 Hz, 2H), 8.30 (d, J = 6.3 Hz, 2H), 8.25 (t, J = 7.6 Hz, 1H), 7.94 (d, J = 8.1 Hz, 2H), 6.54 (s, 1H), 6.31 (s, 2H). HR-ESI-MS (positive scan, *m/z*): $[M+H]^+$ calcd. 731.0773; found 731.1103.

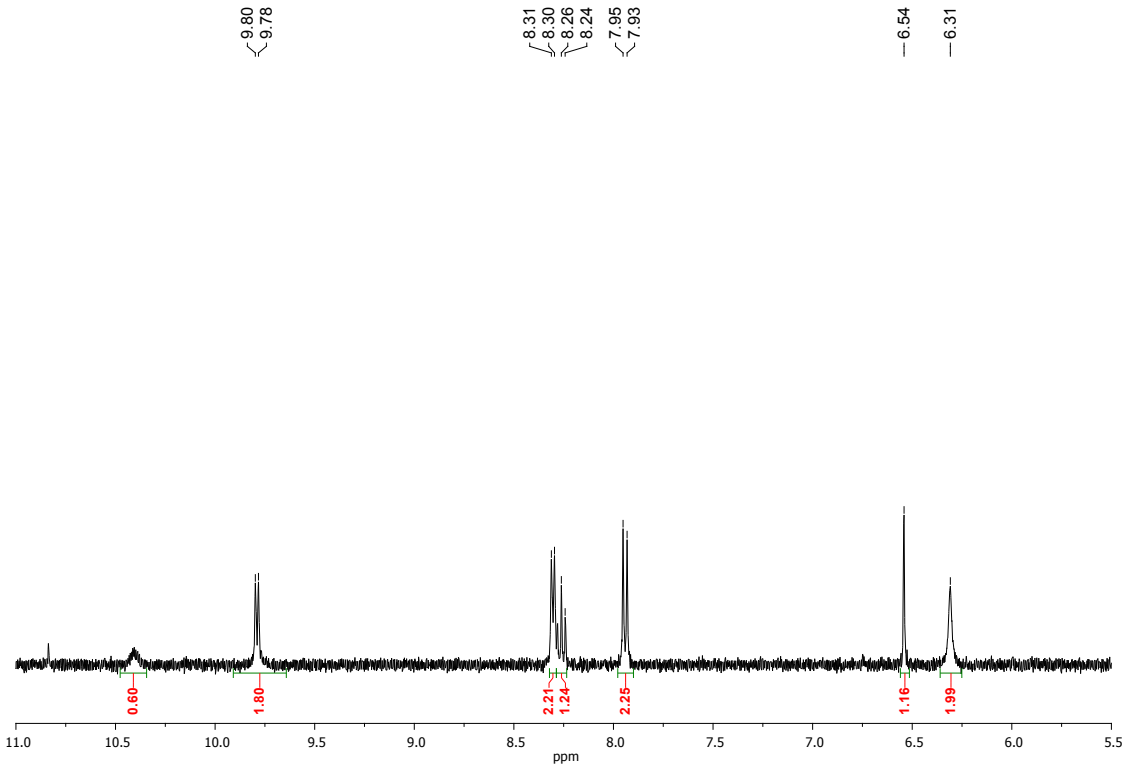

Figure S1: ^{1}H-NMR (400 MHz) spectrum of **CF_3-Pt-Py-iCyt** in THF-d4, zoomed into the aromatic part.

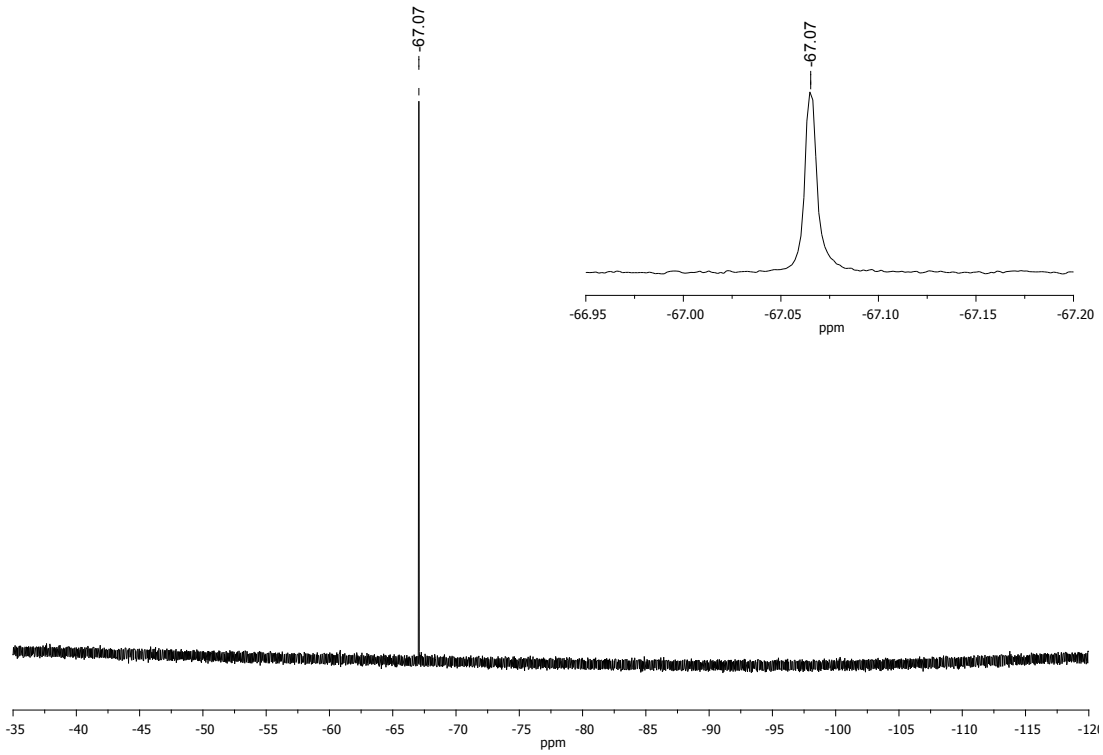

Figure S2: ^{19}F-NMR (377 MHz) spectrum of **CF_3-Pt-Py-iCyt** in THF-d4, inlet shows the zoomed peak.

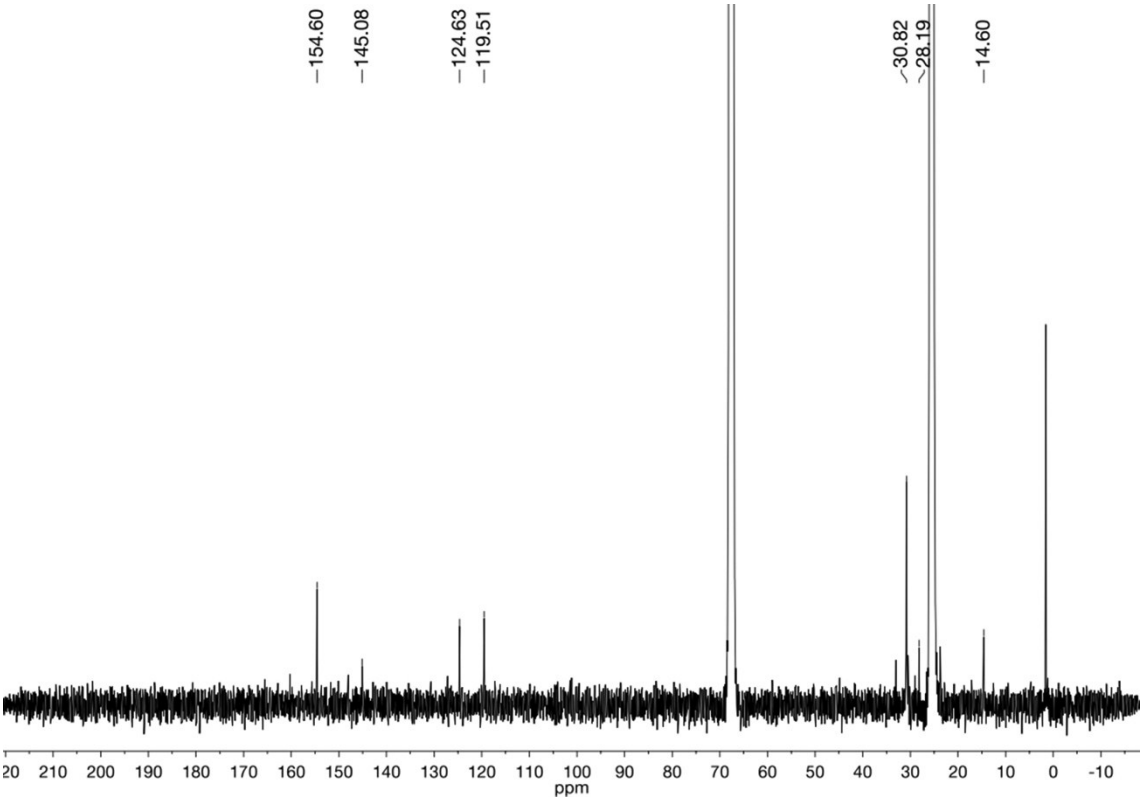

Figure S3: ^{13}C-NMR (101 MHz) spectrum of **CF_3-Pt-Py-iCyt** in THF-d4

2. Photophysical properties

The photophysical properties of the cyclometalated Pt(II) complex **Pt-Py-iCyt** were analysed. In the non-polar solvent, i.e. THF, in which the compound appears molecularly dissolved, strong absorption bands appear in the UV region (216-300 nm) ascribed to as ligand cantered transitions. Featuring a weak MLCT band at 415 nm and an absorption onset of 450 nm the UV-Vis spectrum resembles the typical fingerprint of the **CF_3-Pt-Py**-scaffold[1, 2] accompanied by a pronounced band ranging from 335-368 nm ascribed to π–π* transitions of the pyridine-isocytosine part. (Figure S4) At room temperature a weak structured emission (PLQY<1%) peaking at 462 nm with a short excited-state lifetime of 2.1 ns was observed which is ascribed to be ligand-centered. The solid-state analysis revealed a broad luminescence spectrum centered at 578 nm (Figure S5) arising from a metal-metal-to-ligand-charge-transfer state (^{3}MMLCT) with a prolonged excited-state lifetime (Table S1). The new lowest excited state emerges from aggregation induced closed-shell Pt•••Pt interactions. Unexpectedly, the quantum yield remained very low, which is indicative of a perturbation of the z-directional stacking. The additional rotational axis between the pyridine and the isocytosine moieties as well as the strong intermolecular H-Bond interactions of the latter one may impede the formation of the Pt(II) stacks.

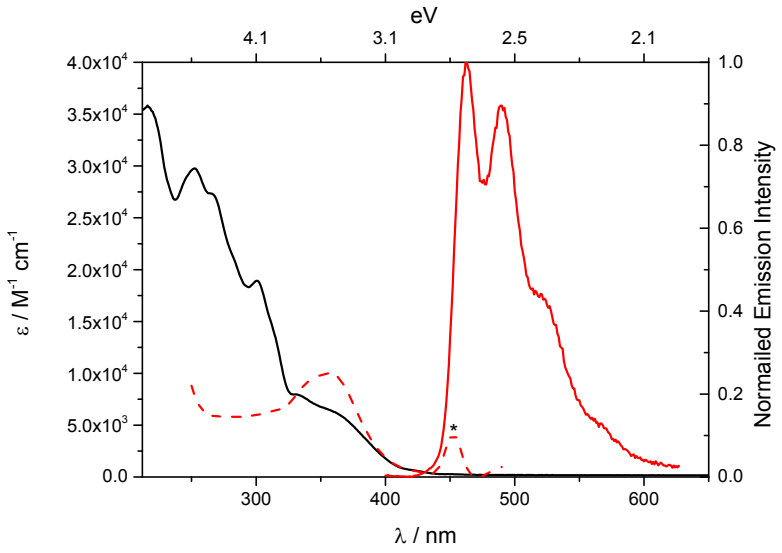

Figure S4. UV/Vis absorption (solid **black**), normalized emission (solid **red**, λ_{ex} = 300 nm) and excitation (dashed **red**, λ_{em} = 460 nm) spectra of **CF_3-Pt-Py-iCyt** in aerated THF (10^{-4} M) at ambient conditions.

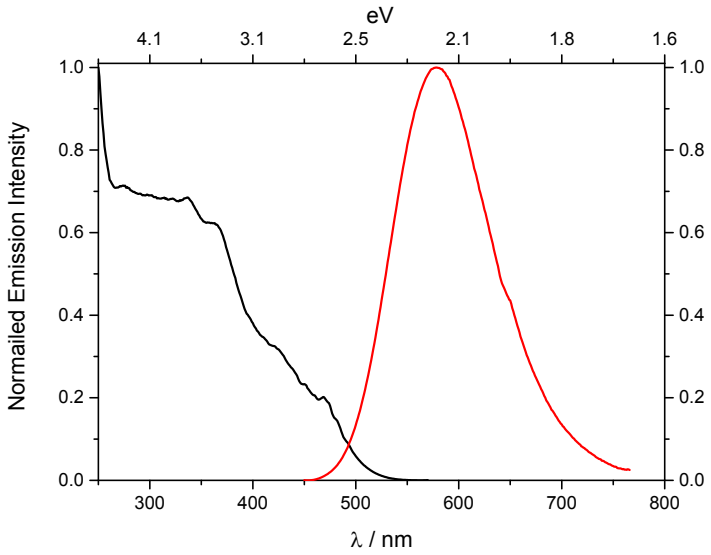

Figure S5. Normalized excitation (**black**, λ_{em} = 600 nm) and emission (**red**, λ_{ex} = 300 nm) spectra of **Pt-Py-iCyt**, in solid state (neat film) at ambient conditions.

Table S1*: Summary of the photophysical properties of the discussed compound.*

	solution THF (10^{-4} M)				***solid state***		
compound	*λ / nm (ε / $M^{-1}cm^{-1}$)*	*$\lambda^{Em\,a}$ /nm*	*PLQY [b]*	*τ/ns [c,d]*	*$\lambda^{Em\,a}$ /nm*	*PLQY [b]*	*τ/ns [c,e]*
CF_3-Pt-PyiCyt	216 (35835), 252 (29758), 267 sh (27243), 300 (18913), 335 (7806), 368 (5714), 415 (785)	462, 489, 517	<1%	2.1	578	< 1%	795 (22%), 265 (45%) 46 (33)%

[a] λ_{ex}=300 nm. [b] Average of scanning λ_{ex}=300–400 nm (10 nm interval), [c] λ_{ex}=375 nm. [d] λ_{em}=462 nm, [e] λ_{em}=578 nm

3. Scanning Tunneling Microscopy

3.1 Experimental section

Scanning Tunneling Microscopy (STM) measurements were carried out by using a Veeco scanning Tunneling microscope (multimode Nanoscope III, Veeco) at the interface between a highly oriented pyrolitic graphite (HOPG) substrate and a supernatant solution, thereby mapping a maximum area of 1 μm × 1 μm. Solution of molecules were applied to the basal plane of the surface. For STM measurements, the substrates were glued to a magnetic disk and an electric contact was made with silver paint (Aldrich Chemicals). The STM tips were mechanically cut from a Pt/Ir wire (90/10, diameter 0.25 mm). The raw STM data were processed through the application of background flattening and the drift was corrected using the underlying graphite lattice as a reference. The lattice was visualized by lowering the bias voltage to 20 mV and raising the current up to 65 pA. STM imaging was carried out in

constant height mode without turning off the feedback loop, to avoid tip crashes. All of the molecular models were minimized with MMFF and processed with QuteMol visualization software (http://qutemol.sourceforge.net).

3.2 Self-assembly of Pyridine-isocytosine

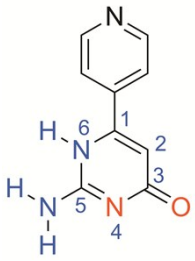

Figure S6. Chemical structure of Pyridine-isocytosine (**Py-iCyt**). Hydrogen-bonding donor and acceptor sites are indicated with red and blue respectively

A drop of (500 ± 2) μM solution of **Py-iCyt** (Figure S6) in 1-phenyloctane was applied to a freshly cleaved graphite surface. The STM was used to probe the self-assembly of **Py-iCyt** molecule at solution-graphite interface. As shown in the figure S8, the network consists of a lamellar pattern that is stable for several hours. The different contrast shown on the STM image of **Py-iCyt** monolayer is a moiré pattern that is caused by electronic mismatch/interferences of the supramolecular adsorbed lattice and the underlying graphite surface. The pattern reveals 2D polycrystalline structure appearing as a ribbon-like architecture (Figure S8). The unit cell parameters are $a=1.24 \pm 0.1$ *nm*, $b = 1.68 \pm 0.1$ *nm* and $\alpha = (60 \pm 2)°$ leading to a surface of $A= (1.80 \pm 0.11)$ *nm*^{2}. The model of the packing within the monolayer is displayed in the Figure S8(b). The structure is stabilized by weak hydrogen bonds occurring between N(4)···H(5) and weak electrostatic interaction formed between O(3), H(5) and H(6) of adjacent molecules (c.f Figure S6 ad Figure S8(c)).

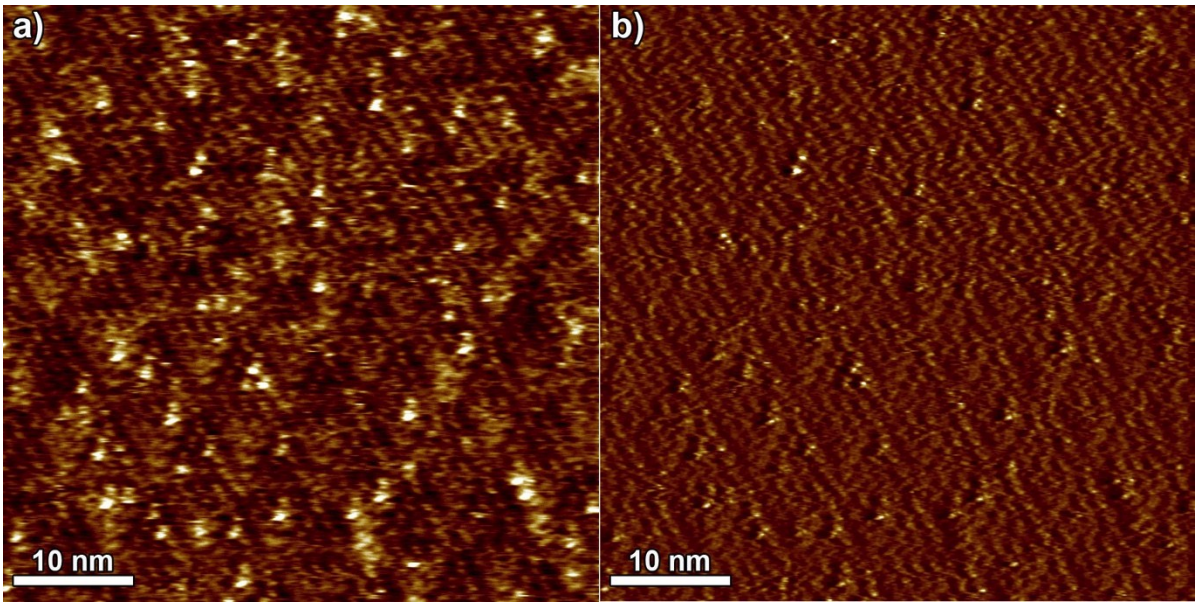

Figure S7. Height (a) and current (b) STM image of **Py-iCyt** monolayer at the 1-phenyloctane/HOPG interface. Scanning parameters, average tunnelling current (I_t) = 20 pA, tip bias voltage (V_t) = 500 mV.

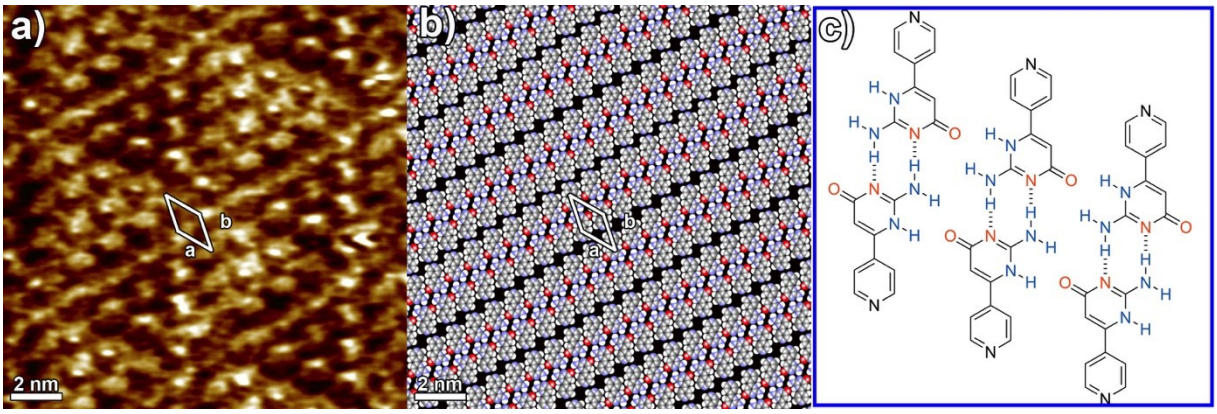

Figure S8. a) Zoom-in of STM image showing the structure of **Py-iCyt** self-assembly at the 1-phenyloctane/HOPG interface. Scanning parameters, average tunnelling current (I_t) = 20 pA, tip bias voltage (V_t) = 500 mV. b) packing model. c) Zoom-in into supramolecular motif.

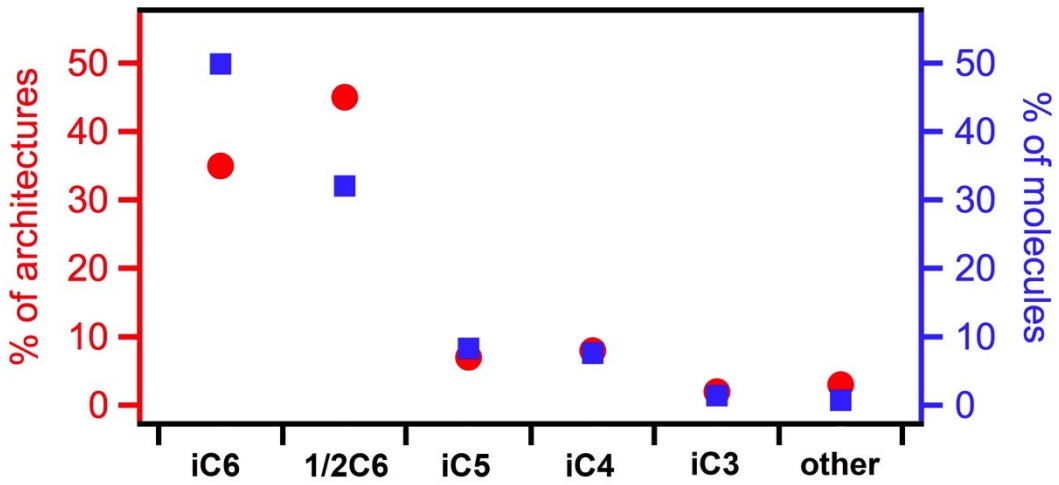

Figure S9. The percentage of the different molecular motifs identified on HOPG surface as well as percentage of molecules involved in formation of a given pattern.

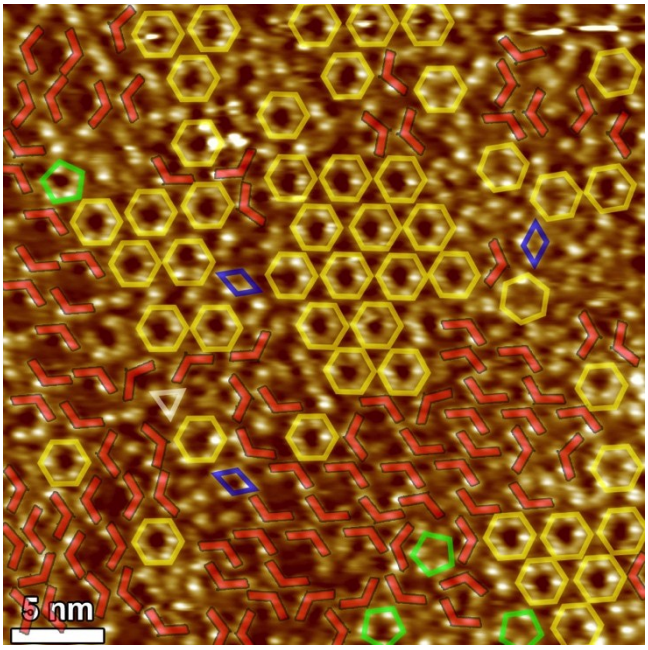

Figure S10. Illustrating the assignment of molecular motifs with STM image.

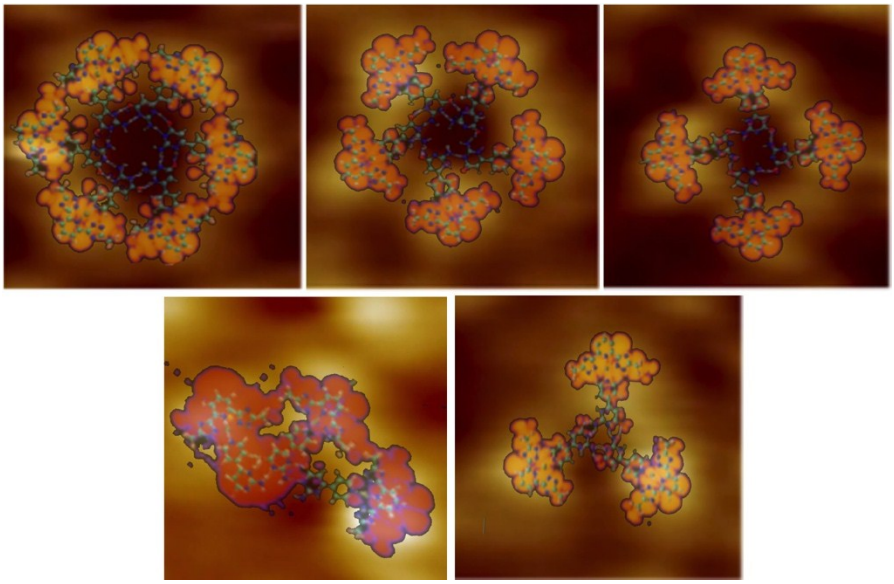

Figure S11. Simulated models overlapping the molecular motifs on the STM images. The models fit vey well the motifs.

4. DFT calculations

4.1 Molecular structures

The computation of stable molecular conformations and the corresponding electronic structure was carried out at the density functional theory (DFT) level of theory with the standard implementation in the CP2K package.

A mixed basis-set approach is used, where the Kohn-Sham orbitals are expanded into linear combinations of contracted Gaussian type orbitals (GTO) and complemented by a plane-wave basis set in order to compute the electronic charge density. In all calculations, the BLYP exchange-correlation functional was used, and its corresponding norm-conserving pseudo-potential GTH (Goedecker, Teter and Hutter). A DZVP (double zeta for valence electrons plus polarization functions) basis set complemented with a plane-wave basis set energy cut-off 350 Ry. Dispersion corrections were included through the standard D3 Grimme parameterization. The convergence criteria for both geometry and energy calculations were set to 1 x 10^{-7} Hartree for the SCF energy and 9 x 10^{-4} (Hartree per Radian). In the case of isolated molecular motifs, calculations were performed with a supercell with box size of 50 × 50 × 20 $Å^3$. These dimensions ensure us to avoid spurious interactions between neighbouring cells when implementing periodic boundary conditions. The different molecular motifs have been constructed partly based on the experimentally observed assemblies visualized with STM, and partly on structural optimization of several

additional motifs. In such way we converged to the supramolecular structures displayed in Figure S12.

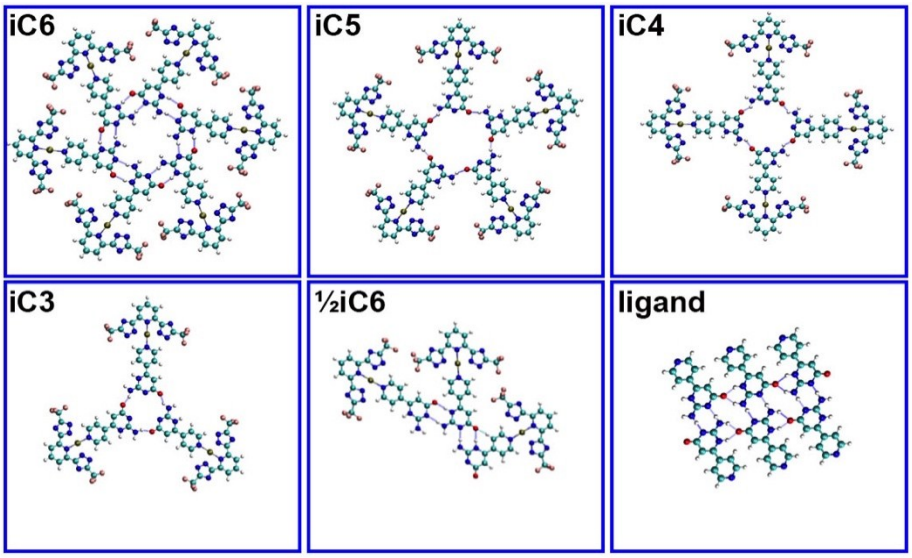

Figure S12. Cyclic molecular motifs of **CF_3-Pt- Py-iCyt** and the ligand (**Py-iCyt**) showing the intermolecular interactions

In order to provide insights on the stability of different conformations of the molecular motifs, composed by the same number of molecules, we have calculated the total energy difference between two configurations, i.e. configuration 1, in which two molecules have been removed from iC6 structure, and iC4 structure (configuration 2). The calculated energy difference ($E_{config.1} - E_{config.2}$) has been found to be ~ +0.5 eV. Hence, we can conclude that the energetically most favourable structure is configuration 2 (close iC4 structure). We believe that the energetically most favourable conformations result from a competition between different effects, namely maximization of the hydrogen bonding, minimization of the repulsive interaction, and minimization of the dipole-dipole interaction. These conditions are achieved for a higher symmetrical structure, as is the case of configuration 2.

4.2 Molecular orbitals

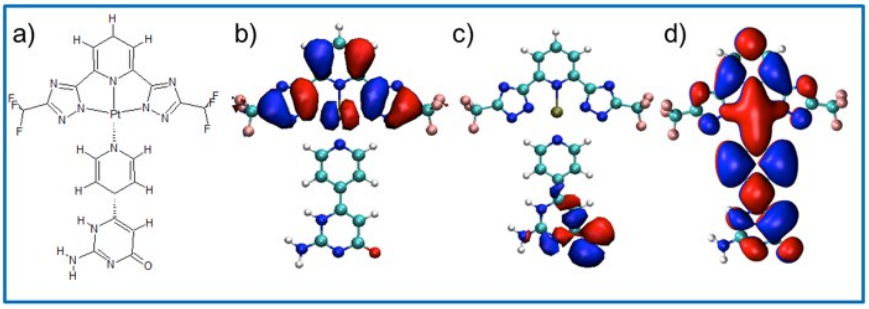

Figure S13. Panels b to d show the HOMO-1, HOMO and LUMO orbitals of the iC molecule. The gap between the HOMO and HOMO-1 states was computed to be 45 meV

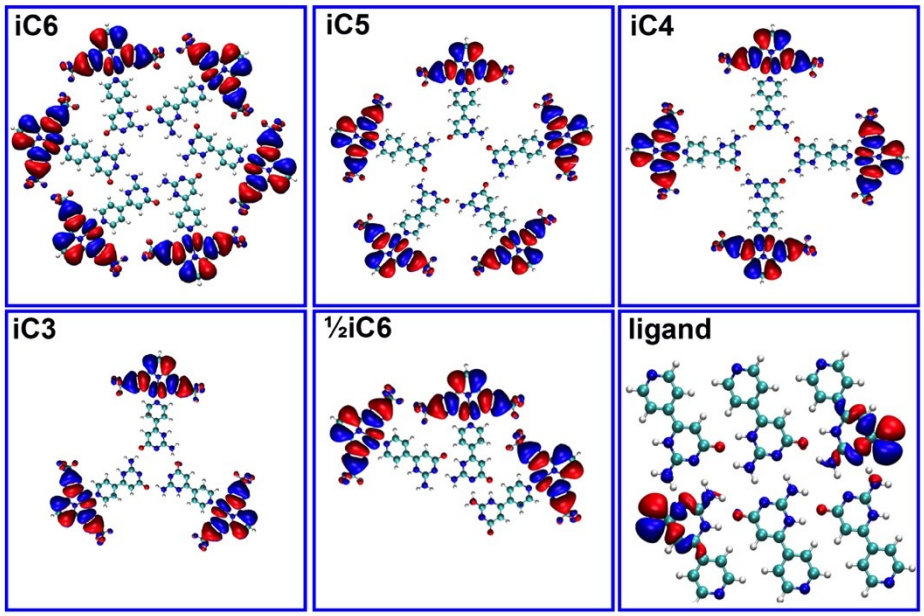

Figure S14. Spatial distribution of the HOMO orbitals of different suggested molecular motifs and a ribbon of ligands (**Py-iCyt**).

4.3 Re-arrangement energies

By the calculation of the dissociation energies of single supramolecular motifs no structural rearrangement of the motif can take place – such as e.g. the transition from conformation iC6 to iC5 – since they are expected to occur over longer time scales not covered by a zero temperature conjugate gradient relaxation algorithm. We have thus defined an additional quantity, the rearrangement energy E_{rearr}, given by the relation:

$$E_{rearr} = E_N - E_{N-1}^{'} - E_{SM} \quad (2)$$

Now, in this expression, E_N refers to the total energy of a supramolecular motif containing N monomers, while the quantity $E_{N-1}^{'}$ is the total energy of a given supramolecular motif with one monomer less, but also with a different spatial symmetry (compare e.g. iC5 and iC6 in Figure S12) differing by one in the number of molecular units. In this sense, E_{rearr} is a measure of the energy required to reorganize the molecular network, while E_{diss} defined in the main text only considers the energy necessary to remove a single monomer without involving a collective rearrangement of the motif, i.e. a change of symmetry.

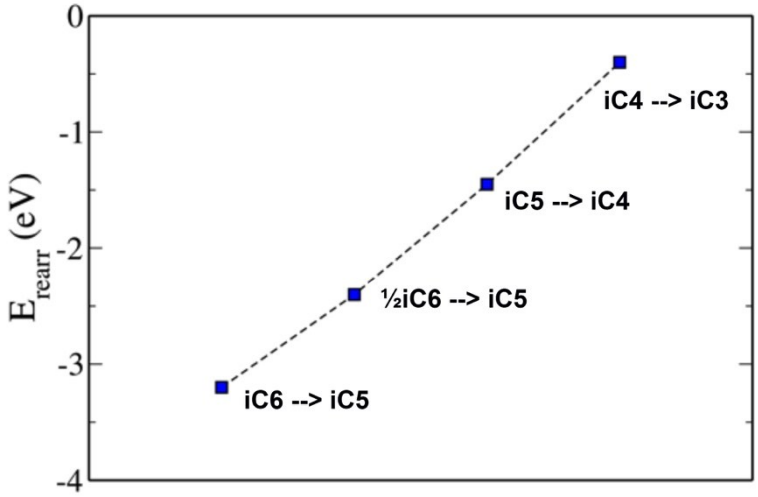

Figure S15. Re-arrangement energy of different molecular motifs formed by the Pt(II) complex. The structures are ranged from iC6 to iC3.

The energy presented in the Figure S15 shows the energy consumption of molecular motifs from iC6 to iC3. Especially, we find rather large energy of transformation from iC6 to iC5 because of the breaking of four H-bonds and rearrangement of the other eight H-bonds. Because of the open structure of ½iC6, the transformation to iC5 needs lower energy compared to the close structure of iC6.

5. References

1. M. Mauro, A. Aliprandi, C. Cebrian, D. Wang, C. Kübel and L. De Cola, *Chem. Commun.*, 2014, **50**, 7269-7272.
2. A. Aliprandi, M. Mauro and L. De Cola, *Nat. Chem.*, 2016, **8**, 10-15.